Published in "Science 338(6107): 666-671, 2012"
which should be cited to refer to this work.

Materials and Methods

Yeast strains and yeast genetic methods. The *S. cerevisiae* strains used in this study are listed in Supplementary Table 3; all strains, unless otherwise specified, are derivatives of W303 (*32*). Deletion disruption and C-terminal tagging were performed as previously described (*33, 34*). Preparation of media, yeast transformation, and genetic manipulations were according to established procedures.

Plasmid constructs. All recombinant DNA techniques were performed according to established procedures using *Escherichia coli* DH5α for cloning and plasmid propagation. All cloned DNA fragments generated by PCR amplification were verified by sequencing. Plasmids used in this study are listed in Supplementary Table 4 and Supplementary Table 5.

Isolation of *rpl5* alleles that are synthetically lethal with *syo1*Δ. Random PCR mutagenesis of *RPL5* was performed as previously described (*35*) and a library of mutant *rpl5*^{mt} alleles was generated by cloning the *rpl5*^{mt} PCR fragments into YCplac111-*RPL5* (*LEU2*). Mutant *rpl5* alleles that are synthetically lethal with the *syo1*Δ null mutant were isolated by a dual screening strategy. Briefly, the *rpl5*^{mt}-library was transformed into a *rpl5*Δ/*syo1*Δ double null mutant strain (relevant genotype: *rpl5*::HIS3MX4, *syo1*::natNT2, *ade2*, *ade3*::kanMX4) containing the plasmids pHT4467Δ-*RPL5* (*ADE3*, *URA3*) and pHT4467Δ(*TRP1*/Δ*URA3*)-*SYO1* (*ADE3*, *TRP1*). Transformants were selected on synthetic dextrose complete (SC)-Leu-Trp plates and colonies were replica plated onto SC+5-FOA-Leu-Trp plates. Growing colonies, bearing viable *rpl5* alleles, were restreaked on SC-Leu plates to identify red, non-sectoring colonies whose growth is dependent on the presence of the *SYO1* plasmid.

Yeast two-hybrid (Y2H) interaction analysis. For Y2H-interaction assays, plasmids expressing bait proteins, fused to the Gal4 DNA-binding domain (G4BD), and prey proteins, fused to the Gal4 activation domain (G4AD), were co-transformed into reporter strain PJ69-4A (*36*). Y2H interactions were documented by spotting representative transformants in 10-fold serial dilution steps onto SC-Trp-Leu, SC-Trp-Leu-His (*HIS3* reporter), and SC-Trp-Leu-Ade (*ADE2*) plates, which were incubated for 3-4 d at 30ºC. Growth on SC-Trp-Leu-His plates is indicative of a weak/moderate interaction, whereas only relatively strong interactions permit growth on SC-Trp-Leu-Ade plates. As a positive control, the combination of plasmids pVA3-1 and pTD1-1 (Clontech) was used; these plasmids also served as negative control when combined with plasmids expressing bait and prey proteins under investigation.

Protein expression, purification, and crystallization. Native and seleno-methionine (Se-Met) labelled *ct*Syo1ΔN23 were expressed in *E. coli* BL21(DE3) (Novagen). *ct*Syo1ΔN23 and *ct*Rpl5(1-41) were co-expressed in *E. coli* BL21(DE3) Rosetta 2. For preparation of native proteins, cells were grown in lysogeny broth medium (LB) at 37ºC under vigorous shaking. Cells expressing *ct*Syo1ΔN23 in Se-Met labelling conditions were grown in M9 medium supplemented with 125 mg lysine, 125 mg threonine, 125 mg phenylalanine, 50 mg valine, 50 mg leucine, 50 mg isoleucine, 5 g glucose, 250 mM $MgCl_2$, 1 mM $CaCl_2$ and 50 mg Seleno-L-methionine per litre. Protein expression was induced at an OD_{600} of approximately 0.6 by the addition of IPTG to 1 mM IPTG. After 3 to 6 h of growth, cells were harvested and stored at -80°C. Cell pellets were resuspended in 10 ml lysis buffer per gram of cells and passed through an M-110L Microfluidizer (Microfluidics). The lysis buffer contained 20 mM HEPES pH 8.0, 350 mM NaCl, 10 mM $MgCl_2$, 10 mM KCl. The lysate was clarified by centrifugation (125'000 g for 30 min at 4ºC) using a Ti-45 rotor (Beckmann) and applied onto a 1 ml HisTrap HP column (GE Healthcare). The column was washed with five column volumes of lysis buffer containing 40 mM imidazole and proteins were eluted in lysis buffer containing 500 mM imidazole. Subsequently, proteins were concentrated and subjected to size-exclusion chromatography using a S200/26–60 column (GE Healthcare) in a buffer containing 20 mM HEPES-Na (pH 7.5), 150 mM NaCl, 10 mM KCl, 10 mM $MgCl_2$.

Crystallization screens were performed at 291 K by the sitting-drop vapour-diffusion method upon mixing equal volumes (0.5 µl) of protein solution (30 mg/ml) and crystallization buffer with a reservoir volume of 100 µl. Crystals of *ct*Syo1 and Se-Met labelled *ct*Syo1ΔN23 appeared within 2-7 d in 0.2 M potassium acetate, 20% (v/v) PEG 3350. Crystals of the *ct*Syo1ΔN23/*ct*Rpl5(1-41) complex appeared within 3-10 d in 0.1 M succinic acid pH 7.0, 20% (v/v) PEG 3350.

Data collection and structure determination. Prior to X-ray analysis, crystals were flash-frozen in liquid nitrogen after cryo-protection by transfer into cryo-solution containing mother liquor and 20% (v/v) glycerol. Diffraction data were measured on the tuneable beamline ID23-1 under cryogenic conditions (100 K; Oxford Cryosystems Cryostream) at the European Synchrotron Radiation Facility (ESRF) in Grenoble, France. X-ray diffraction data were processed using iMosflm (*37*). The initial model of *ct*Syo1 was obtained from a SAD Se-Met dataset of *ct*Syo1ΔN23 using the AutoSol and Autobuild programs of the Phenix program suite (*38*). The structures of *ct*Syo1 and the *ct*Syo1ΔN23/*ct*Rpl5(1-41) complex were obtained by molecular replacement using Phaser (*37*) and the structure of *ct*Syo1ΔN23 as search model. Model building and refinement was performed with the Phenix program suite (*38*) and COOT (*39*). Figures were prepared in PyMOL (http://pymol.org/).

Preparation of 5S rRNA. The DNA encoding 5S rRNA was amplified from genomic DNA of *C. thermophilum*. The sequence of the 5S rDNA from *C. thermophilum* is: 5'-ACGTACGACCATACCCAGTGGAAAGCACGGCATCCCGTCCGCTCTGCCCTAGTTA AGCCACTGAGGGCCCGGTTAGTAGTTGGGTCGGTGACGACCAGCGAATCCCGGG TGTTGTACGTT-3'. The fragment was cloned into pUC18 *via* the *Kpn*I and *Bam*HI restriction sites. The forward primer additionally contained a T7 promoter sequence. The RNA was produced by *in vitro* transcription as described in (*40, 41*). Prior to the biochemical assays, purified 5S rRNA was heated to 75ºC for 10 min and snap-cooled on ice to ensure proper folding.

FG-repeat binding assays. *In vitro* binding assays with immobilized GST-tagged FG-repeats of nucleoporins were performed as described (*27*). BIAcore binding assays and determination of dissociation constants was done as described (*27*).

***In vitro* import assays.** *In vitro* import assays with permeabilized HeLa cells were performed as previously described (*26, 27*). To monitor nuclear translocation by fluorescence microscopy (Axiophot 2 or Axiovert 100M microscope, Zeiss), purified proteins were either fluorescently labelled with Alexa-488 or, when tagged with the Flag epitope, detected with rabbit anti-FLAG (Sigma) and Alexa-488 labelled secondary donkey anti-rabbit (Invitrogen) antibodies. Nuclei were revealed by staining DNA with Hoechst.

Determination of the absolute MW by SLS/RI measurements. The apparent molecular weight was analyzed by size-exclusion chromatography using a S200/26–60 column (GE Healthcare). The buffer was 20 mM Hepes 7.5, 150 mM NaCl, 10 mM MgCl2, and 10 mM KCl. The absolute molecular weight was determined by static light scattering (mini Dawn Tristar; Wyatt Technologies) and refractive index analysis (WGE Dr. Bures Δn1000, Dallgow, Germany).

Amide HDX-MS Experiments. Amide HDX-MS experiments were performed as described (*42, 43*). Amide HDX was initiated by a 20-fold dilution of either 200 pmol *ct*Syo1 or *ct*Syo1-*ct*Rpl11 complex into D_2O buffer containing 20 mM Hepes (pH 7.5), 150 mM NaCl, 10 mM $MgCl_2$, and 10 mM KCl at 30ºC. After 10 sec the exchange reaction was quenched by decreasing the temperature to 0ºC and the pH with ice-cold quench buffer (400 mM KH_2PO_4/H_3PO_4, pH 2.2). Quenched samples were digested with pepsin and then injected into an HPLC-MS setup as described. The deuteron content of the peptic peptides covering the *ct*Syo1 or *ct*Syo1-*ct*Rpl11 complex were determined from the centroid of the molecular ion isotope envelope. The deuteron content was calculated after adjustment for deuteron gain/loss

during digestion and HPLC-MS setup. For this adjustment, nondeuterated and fully deuterated *ct*Syo1 were analyzed (*44*). Fully deuterated samples were prepared by 3 cycles of drying and resolubilization in D_2O containing 6 M guanidium hydrochloride. The 0% control was not treated with D_2O.

Miscellaneous. Polysome profiles were analysed by sucrose gradient centrifugation as previously described (*45*, *46*). Tandem-affinity purifications were, unless otherwise indicated, performed in a buffer containing 50 mM Tris-HCl pH 7.5, 100 mM NaCl, 5 mM $MgCl_2$, 5% glycerol, and 0.1% NP-40 as previously described (*46*). Elution from Calmodulin-Sepharose beads (GE Healthcare) was performed in the presence of 5 mM EGTA and elution from anti-FLAG M2 affinity gel (Sigma) was carried out by incubation with 0.1 mg/ml FLAG peptide. Standard methods were used to purify $(His)_6$- or GST-tagged proteins from *E. coli*. Recombinant proteins were revealed by Western analysis with mouse monoclonal anti-FLAG M2 (Sigma) or anti-penta-His (Qiagen) antibodies and secondary goat anti-mouse horseradish peroxidase conjugated antibodies (Bio-Rad). Live yeast cells were imaged by fluorescence microscopy using either a Zeiss Imager Z1 or an Olympus BX54 microscope.

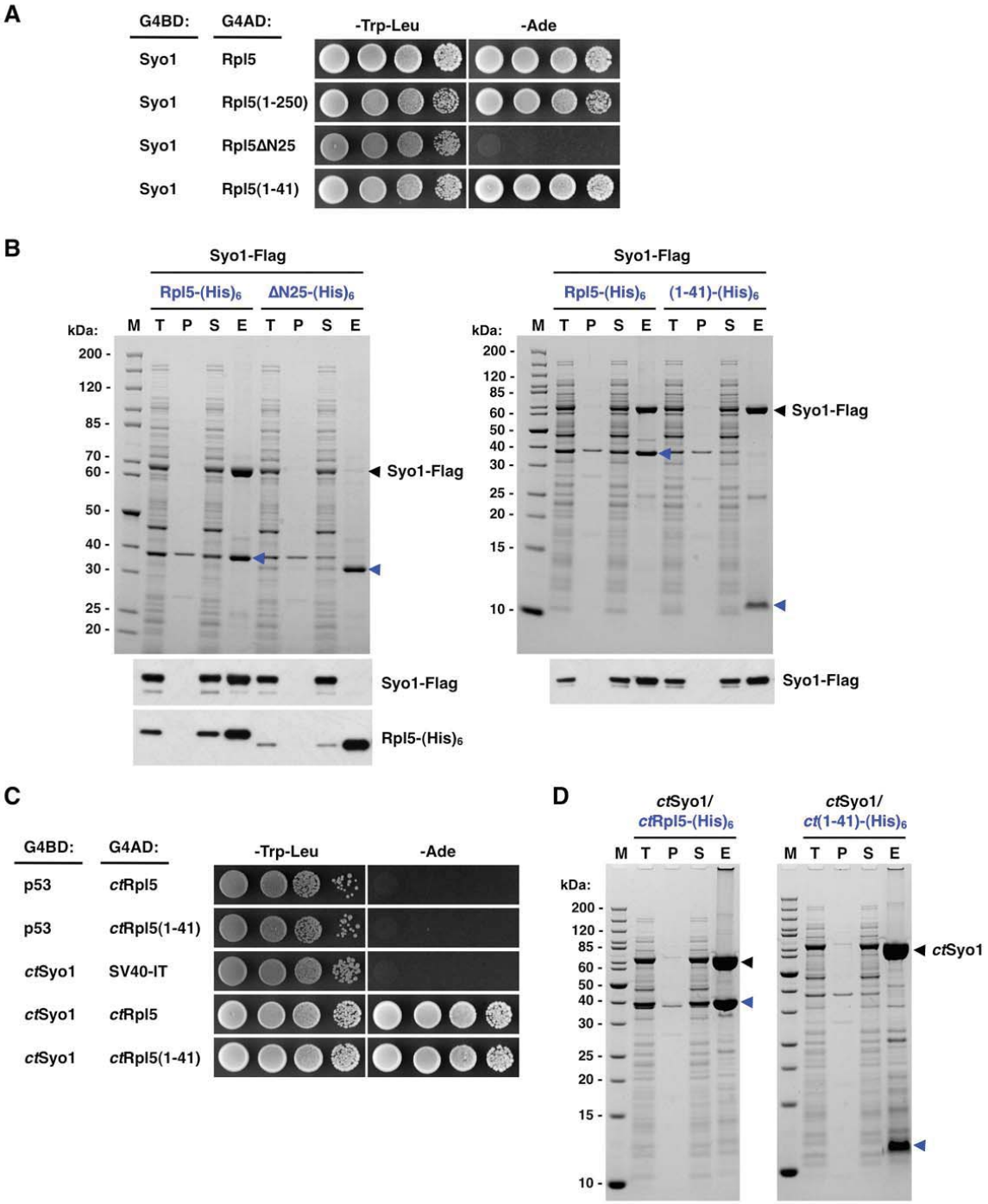

Fig. S1. Syo1 binds to the N-terminal extension of Rpl5. **(A, B)** The N-terminal extension of Rpl5 is required and sufficient for the interaction with Syo1. **(A)** Mapping of the Syo1 binding site on Rpl5 by Y2H-interaction assay. The Rpl5(1-250) construct lacks the C-terminal extension of Rpl5. The Rpl5ΔN25 construct lacks the first 25 amino acids of Rpl5 and begins with glycine 26. **(B)** *In vitro* binding assay between Syo1 and Rpl5. Syo1-Flag and the indicated C-terminally $(His)_6$-tagged Rpl5 variants were co-expressed from pETDuet-1 (Novagen). Proteins, purified *via* Nickel-ion affinity chromatography, were eluted with 250 mM imidazole and revealed by SDS-PAGE and Coomassie staining (upper panels) or by Western analysis using anti-FLAG (Syo1-Flag) and anti-penta-His (Rpl5-$(His)_6$ variants)

antibodies (lower panels). The buffer used for the purification had the following composition: 50 mM Tris-HCl pH 7.5, 200 mM NaCl, 1.5 mM $MgCl_2$, 5% glycerol, and 0.1% NP-40. T, total extract; P, pellet fraction (insoluble proteins); S, soluble extract; E, eluate; M, molecular weight standard. The bands marked by a blue arrowhead correspond to the different Rpl5 variants used as baits for the purifications. Black arrowheads indicate the position of Syo1-Flag. **(C, D)** The N-terminal extension of *ct*Rpl5 is sufficient for the interaction with *ct*Syo1. **(C)** Y2H-interaction assay between *ct*Syo1 and *ct*Rpl5 or *ct*Rpl5(1-41). **(D)** *In vitro* binding assay between *ct*Syo1 and *ct*Rpl5 or *ct*Rpl5(1-41). Black and blue arrowheads indicate *ct*Syo1 and *ct*Rpl5-$(His)_6$ or *ct*Rpl5(1-41)-$(His)_6$, respectively. M, molecular weight standard.

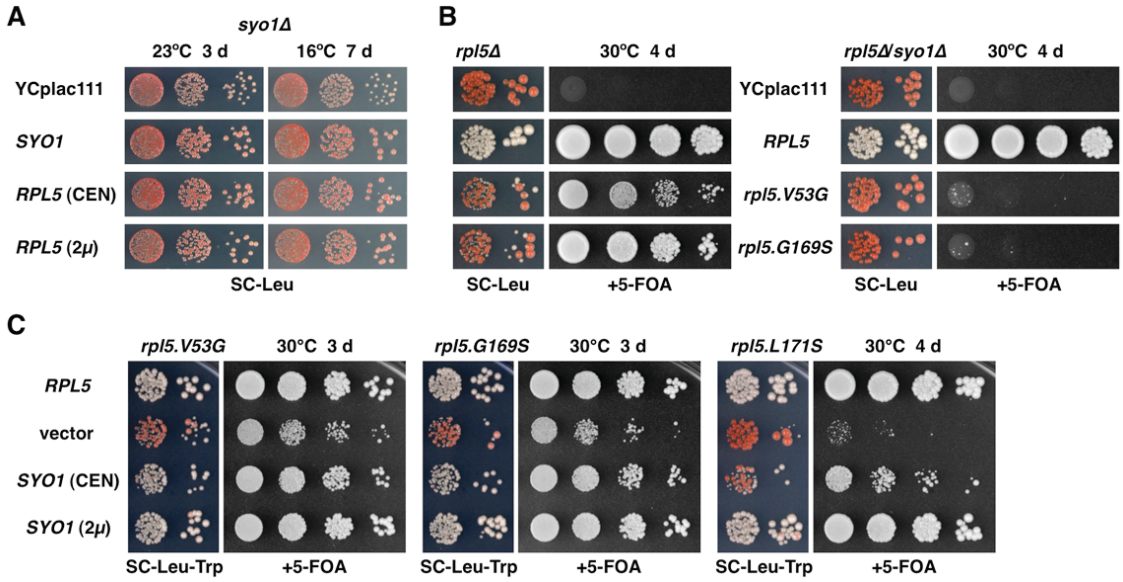

Fig. S2. Syo1 and Rpl5 functionally interact. **(A)** Increased dosage of Rpl5 suppresses the *syo1*Δ null mutant phenotype. The *syo1*Δ null mutant was transformed with YCplac111, YCplac111-*SYO1*, YCplac111-*RPL5*, and YEplac181-*RPL5*. Transformants were restreaked and cells were spotted in 10-fold serial dilution steps onto SC-Leu plates, which were incubated at 23ºC for 3 d or at 16ºC for 7 d. CEN, centromeric plasmid; 2*μ*, multicopy plasmid. **(B)** The *syo1*Δ null mutant is synthetically lethal with distinct *rpl5* alleles. YCplac111, YCplac111-*RPL5*, YCplac111-*rpl5.V53G*, and YCplac111-*rpl5.G169S* were transformed into a *RPL5* shuffle strain (*rpl5*::HIS3MX4 *ade3*::kanMX4 pHT4467Δ-*RPL5*) and a *RPL5/syo1*Δ shuffle strain (*rpl5*::HIS3MX4 *syo1*::natNT2 *ade3*::kanMX4 pHT4467Δ-*RPL5*). Transformants were restreaked and cells were spotted in 10-fold serial dilution steps onto SC-Leu and SC+5-fluoroorotic acid (5-FOA) plates, which were incubated at 30ºC for 4 d. The *rpl5.V53G* allele has originally also been described as *rpl5-HA-3* (*47*). Note that the other published, viable *rpl5* alleles (*HA-1*, *HA-2*, *HA-4*, *HA-5*, and *HA-9*) are not synthetically lethal with the *syo1*Δ null mutant (data not shown). **(C)** Overexpression of Syo1 rescues the slow-growth phenotypes of *rpl5* alleles. YCplac22, YCplac22-*RPL5*, YCplac22-*SYO1*, and YEplac112-*SYO1* were co-transformed with YCplac111-*rpl5.V53G*, YCplac111-*rpl5.G169S* or YCplac111-*rpl5.L104S* into a *RPL5* shuffle strain. Transformants were restreaked and cells were spotted in 10-fold serial dilution steps onto SC-Leu-Trp and SC+5-FOA plates, which were incubated at 30ºC for 3 d or 4 d.

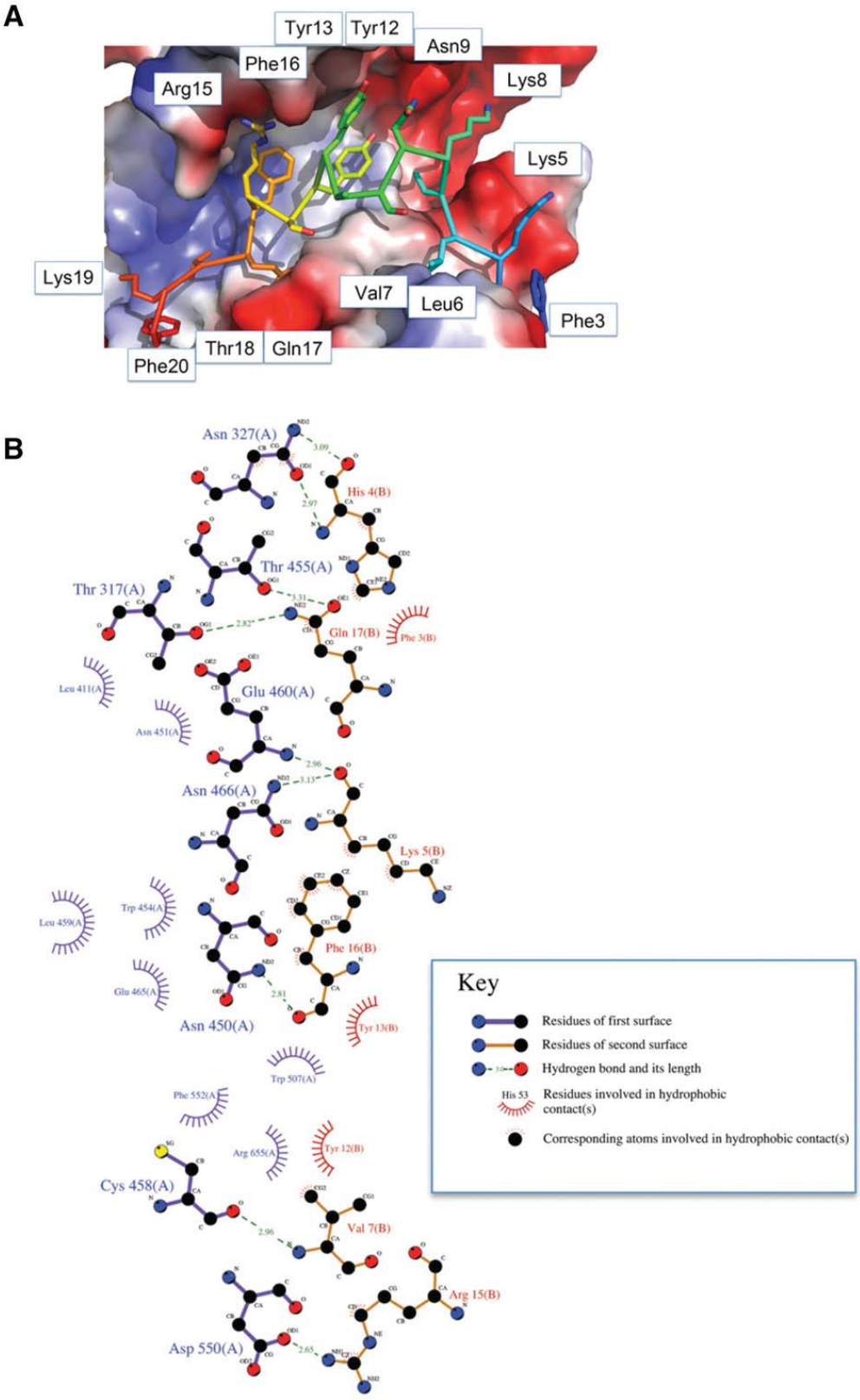

Fig. S3. Interaction of L5-N with *ct*Syo1. (**A**) Residues of L5-N involved in binding to *ct*Syo1, of which the electrostatic surface is shown. L5-N binds into an elongated, hydrophobic groove, which is lined by electrostatic residues. (**B**) Residues of *ct*Syo1

involved into L5-N binding. The Figure was created with Ligplot. Note: Arg15 of L5-N might be further involved in two potential salt bridges with Asp550 and Glu651 of *ct*Syo1.

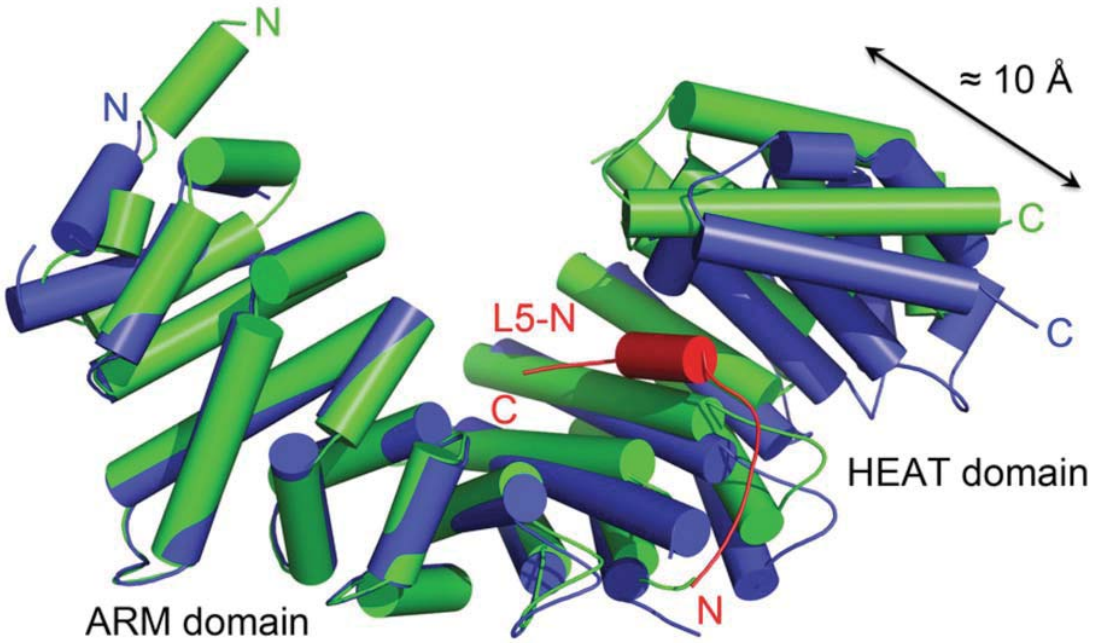

Fig. S4. Conformational rearrangements of *ct*Syo1 upon L5-N binding. The crystal structures of *ct*Syo1 (green) and *ct*Syo1 (blue) bound to L5-N (red) were superimposed on their ARM domains (rmsd = 2,2 Å). The comparison shows that the HEAT domain of *ct*Syo1 is translated for approximately 10 Å relatively to the ARM domain.

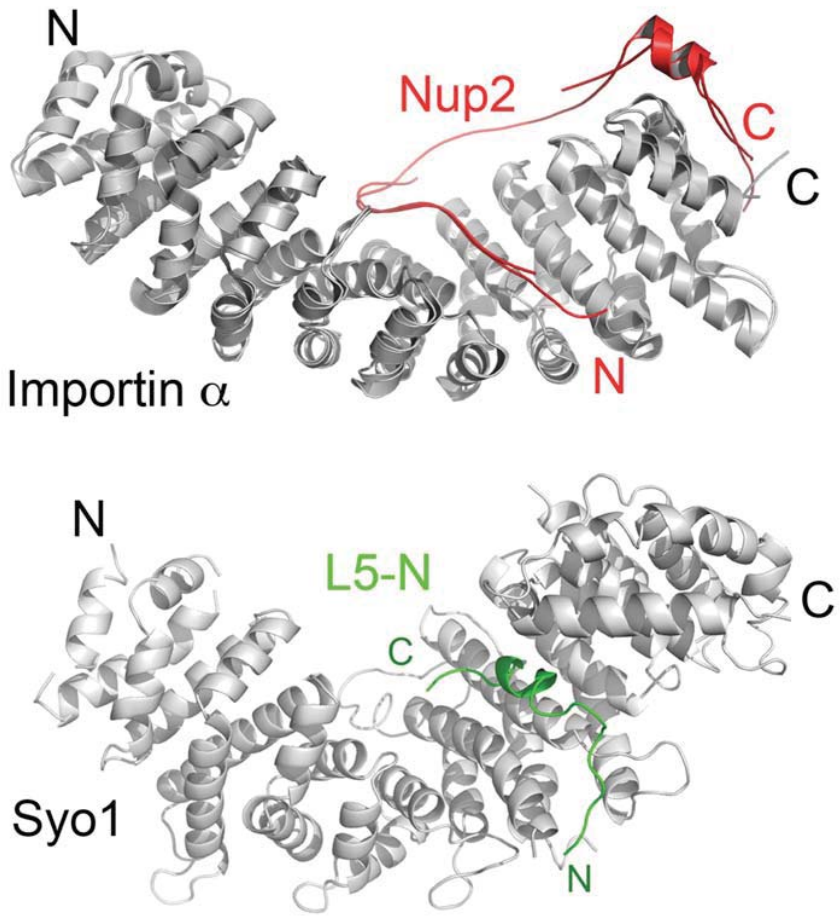

Fig. S5. Comparison of the ligand-binding mode between importin-α and *ct*Syo1. (**A**) Superposition of two structures of importin-α (grey) in complex with Nup2 (red, PDB: 2C1T (*24*) or PDB: 3TJ3). (**B**) Equivalent view of the structure of *ct*Syo1 (grey) in complex with L5-N (green) (this study).

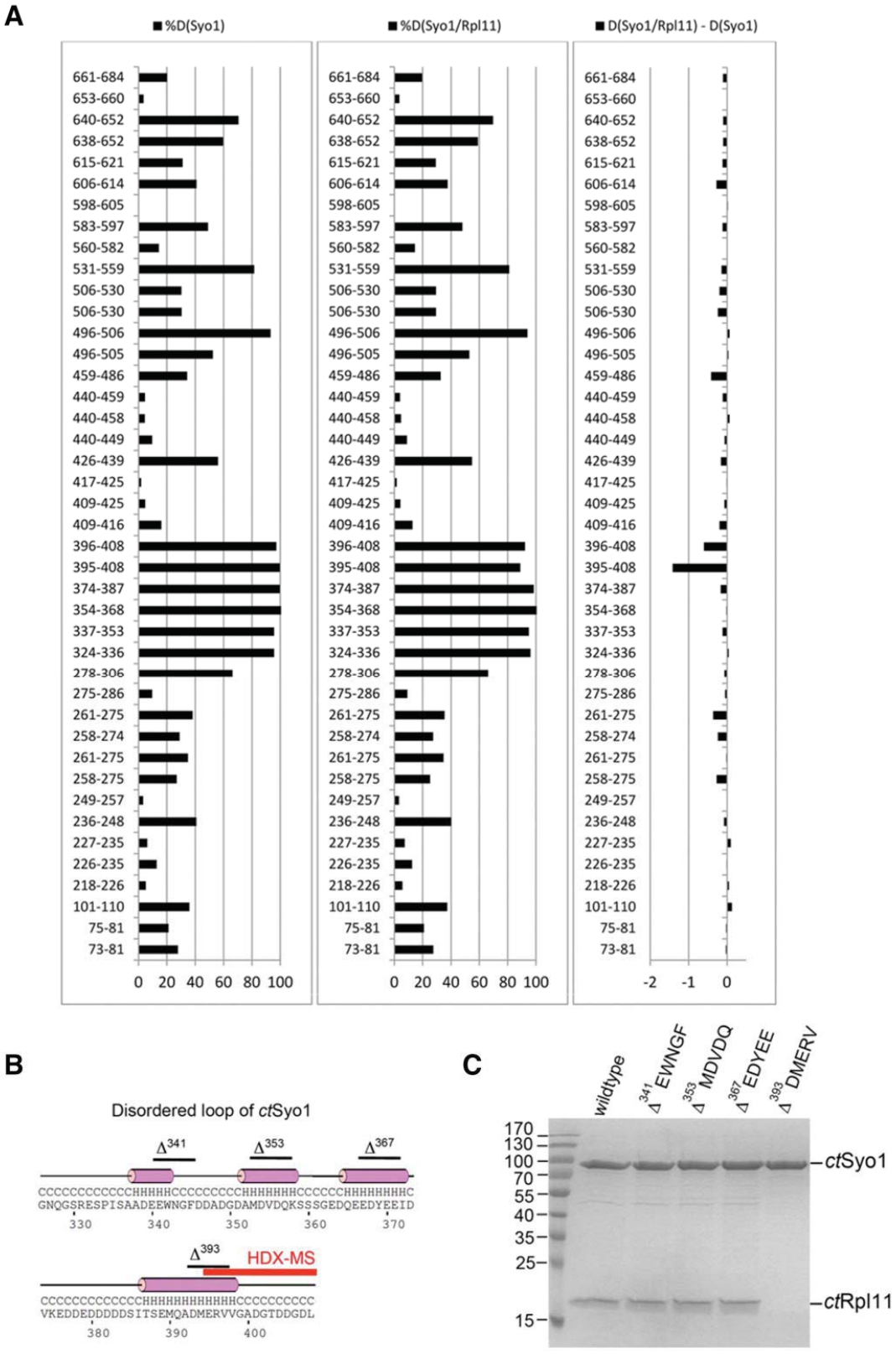

Fig. S6. Analysis of *ct*Syo1/Rpl11 interaction: Part of the *ct*Syo1 acidic loop contributes to *ct*Rpl11 binding. **(A)** Mapping of the *ct*Rpl11 binding sites on *ct*Syo1 by HDX-MS analysis.

Deuteron incorporation into uncomplexed Syo1 (left panel) and *ct*Syo1 bound to *ct*Rpl11 (middle panel) after 10 sec of incubation in D_2O. Results are shown as fraction exchanged in % of total exchangeable amides in the particular peptide. The numbers corresponding to the protein segments (peptides) are indicated on the left. Difference plot of the number of deuterons incorporated into the *ct*Syo1-*ct*Rpl11 complex compared to free *ct*Syo1 (right panel). In the difference plot, bars to the left indicate *ct*Rpl11-induced protection in Syo1 (less deuteron incorporation). (**B**) Sequence of the *ct*Syo1 disordered loop and secondary structure prediction with Psipred (*48*). The black and red bars indicate the positions of the generated 5 amino acid deletions in *ct*Syo1 and the major binding site of *ct*Rpl11 on *ct*Syo1 as identified by HX-MS, respectively. (**C**) *In vitro* binding assay between *ct*Syo1 and its variants and *ct*Rpl11. Proteins were co-expressed in *E. coli*, purified *via* Nickel-ion affinity purification and revealed by SDS-PAGE and Coomassie staining.

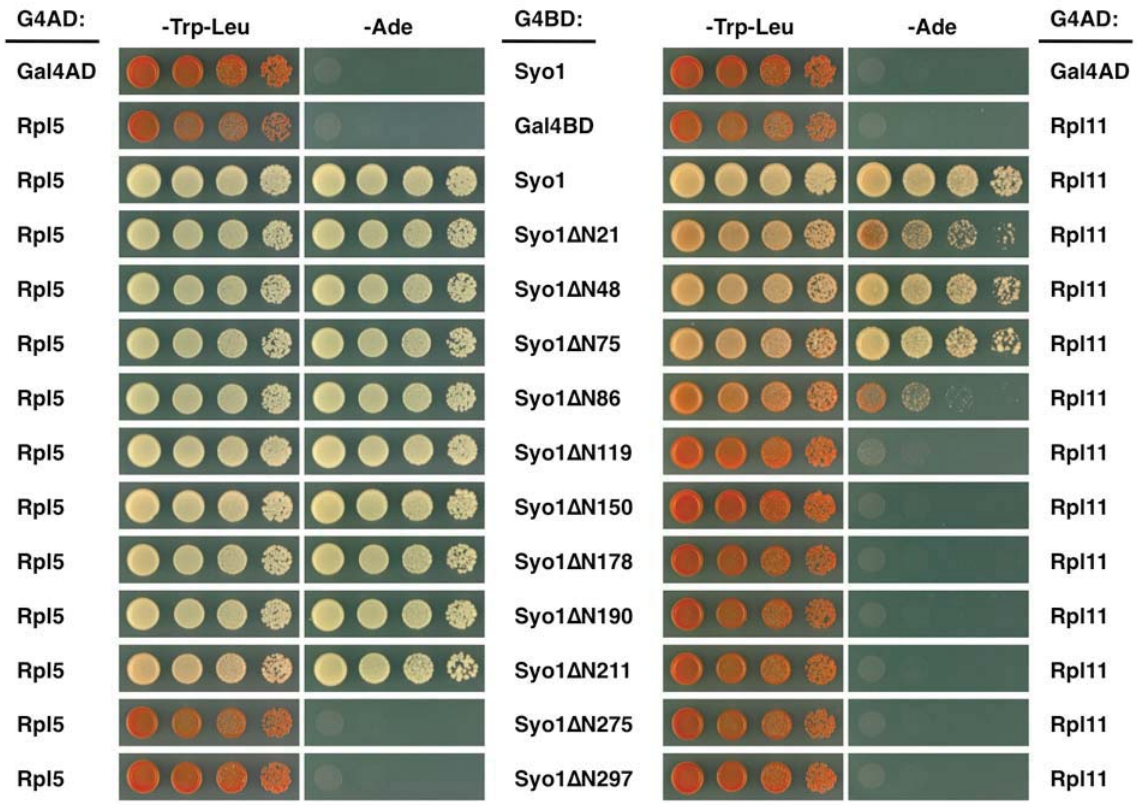

Fig. S7. The ARM-repeat domain of Syo1 contributes to Rpl11 binding. Mapping of the Rpl5 and Rpl11 binding sites on Syo1 by Y2H-interaction assay. Progressive N-terminal deletion constructs of Syo1 were tested for their interaction with full-length Rpl5 and Rpl11, respectively.

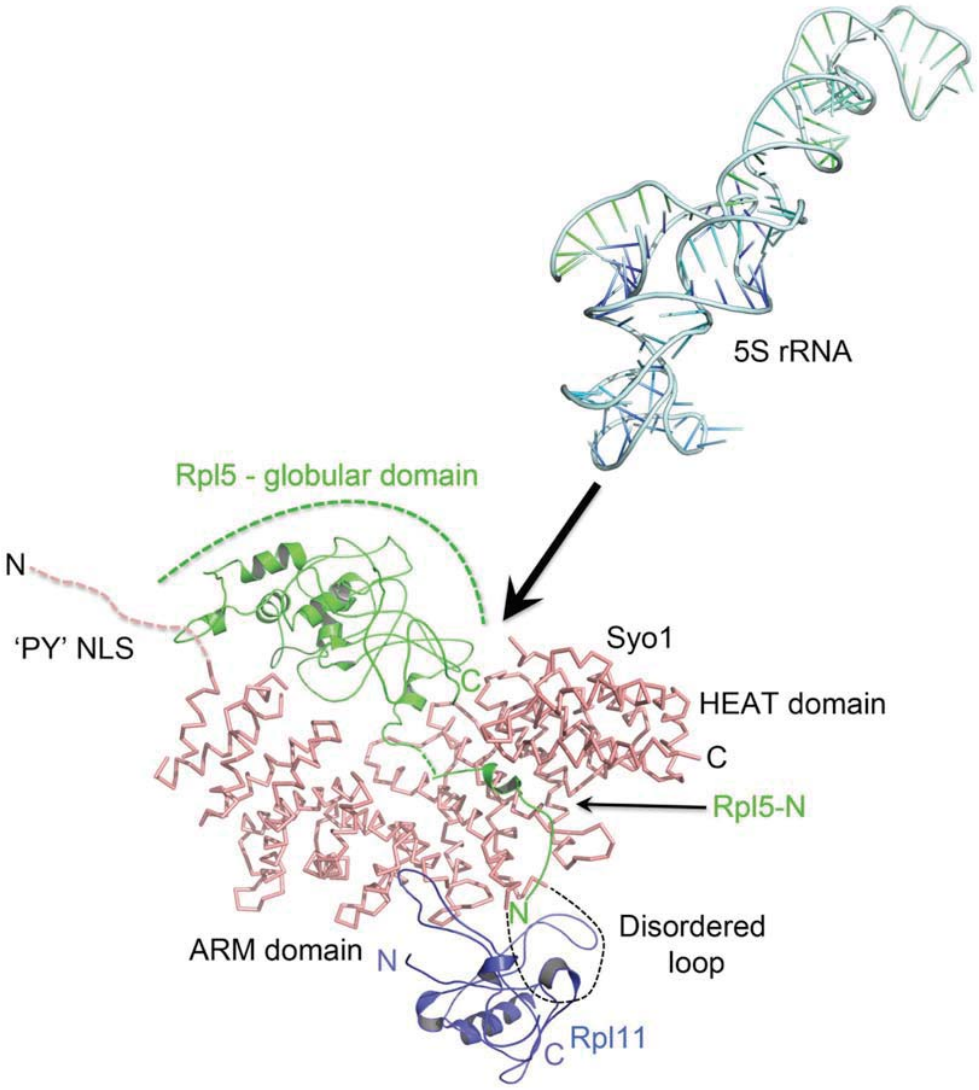

Fig. S8. Possible domain organisation of the Syo1-Rpl5-Rpl11 complex. The basis for this illustration is the crystal structure of *ct*Syo1 (salmon) in complex with L5-N. The globular domain of Rpl5 (green) was taken from the crystal structure of the 80S ribosome from *S. cerevisiae* (*13*) and arbitrarily placed following the L5-N peptide (see 'green dashed line'). Rpl11 (blue) was placed in close proximity to the disordered loop of Syo1 (black dashed lines), which provides a key interaction site (see fig. S6). As a consequence, Rpl11 would likely contact the ARM domain of Syo1, which is also involved in the Syo1/Rpl11 interaction (see fig. S7). Note: The intention of the figure is to provide an idea about the relative protein sizes and a possible domain arrangement. It is not meant as a precise molecular model of the Syo1-Rpl5-Rpl11 complex. With this intention, the authors also included the structure of the 5S rRNA as observed in the 80S ribosome (*13*). The arrow indicates the direction how the 5S rRNA could 'meet' the Syo1-Rpl5-Rpl11 complex to form the stable complex described in Fig. 4.

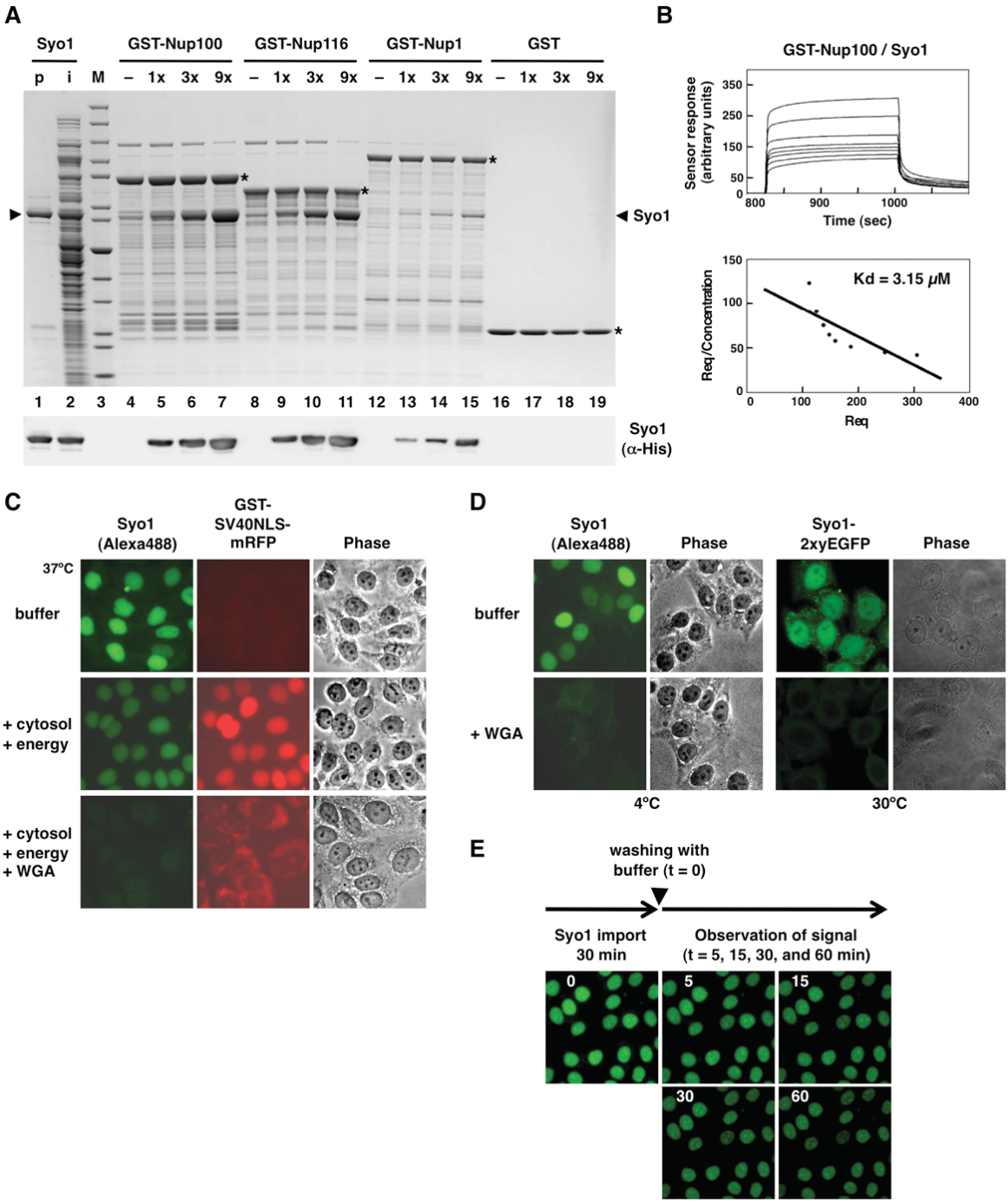

Fig. S9. Syo1 traverses the NPC by facilitated diffusion. **(A, B)** Syo1 interacts with FG-repeats of nucleoporins. **(A)** Binding of recombinant Syo1 to immobilized FG-repeat domains of nucleoporins (GST-Nup) in the presence of competitor *E. coli* lysate. Lane 1, purified Syo1 (p); lane 2, Syo1 mixed with *E. coli* lysate (input, i); lane 3, molecular weight standard (M), same as in Fig. S1B; lanes 4-19, proteins bound to the indicated GST-Nups or the GST control in the absence (-) or presence of increasing amounts of Syo1 (1x, 3x, 9x). Bound proteins were analyzed by SDS-PAGE and Coomassie staining (upper panel) or Western analysis (lower panel) with anti-penta-His antibody (Syo1). **(B)** BIAcore analysis of the interaction between Syo1 and the FG-repeat domain of Nup100. GST-Nup100 was

immobilized and different concentrations (0.91 - 7.28 μM) of purified Syo1 were injected over the sensor chip. The dissociation constant (Kd) for Syo1 binding to FG-repeats of Nup100 was determined by Scatchard analysis. Sensor responses at equilibrium (R_{eq}) were derived for each protein concentration from the sensorgram, and R_{eq}/concentration of Syo1 values were plotted as a function of R_{eq}. **(C, D)** *In vitro* nuclear import assays. HeLa cells were permeabilized by digitonin and incubated with purified, Alexa488-labelled Syo1 or GST-SV40NLS-mRFP in transport buffer (**C**, upper panel), transport buffer containing either cytosol/energy (**C**, middle panel) or cytosol/energy/WGA (**C**, lower panel) at 37ºC. Permeabilized HeLa cells were pre-treated with transport buffer containing cytosol/energy in the absence or presence of WGA before performing the import reactions. **(D)** *In vitro* import assay with purified, Alexa488-labelled Syo1 at 4ºC in the absence or presence of WGA (left panel) and with purified Syo1-2xyEGFP at 30ºC in the absence or presence of WGA (right panel). **(E)** Syo1 can re-equilibrate across the NPC after nuclear accumulation. Permeabilized HeLa cells were incubated with purified, Alexa488-labelled Syo1 in transport buffer, then cells were washed with buffer (t = 0) and the Syo1 signal was monitored over time (t = 5, 15, 30, and 60 min). At longer time points, the nucleoplasmic signal of labelled Syo1 is clearly reduced, while a fraction of Syo1 remains associated with sub-nuclear regions that likely correspond to nucleoli.

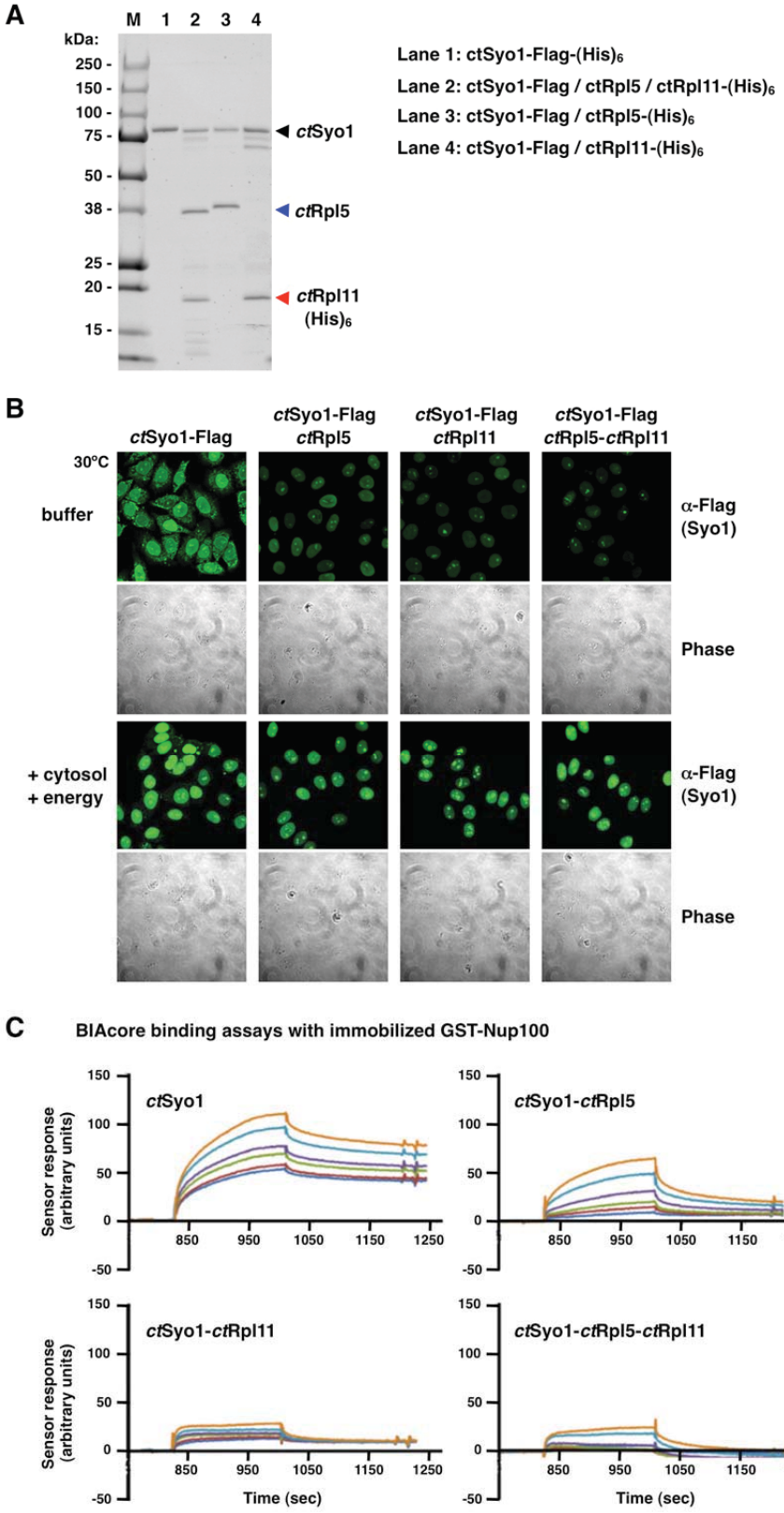

Fig. S10. *In vitro* nuclear import assays and BIAcore FG-binding assays with *ct*Syo1, *ct*Syo1-*ct*Rpl5, *ct*Syo1-*ct*Rpl11 and *ct*Syo1-*ct*Rpl5-*ct*Rpl11. **(A)** Protein input for import and

BIAcore assays. *ct*Syo1-Flag-$(His)_6$ (lane 1), *ct*Syo1-Flag/*ct*Rpl5/*ct*Rpl11-$(His)_6$ (lane 2), *ct*Syo1-Flag/*ct*Rpl5-$(His)_6$ (lane 3), and *ct*Syo1-Flag/*ct*Rpl11-$(His)_6$ (lane 4) were purified *via* Nickel-ion affinity chromatography and analyzed by SDS-PAGE and Coomassie staining. Black, blue, and red arrowheads indicate *ct*Syo1-Flag/*ct*Syo1-Flag-$(His)_6$, *ct*Rpl5/*ct*Rpl5-$(His)_6$, and *ct*Rpl11-$(His)_6$, respectively. M, molecular weight standard. **(B)** *In vitro* nuclear import assays. HeLa cells were permeabilized by digitonin and incubated with purified *ct*Syo1 or the *ct*Syo1-*ct*Rpl5, *ct*Syo1-*ct*Rpl11, and *ct*Syo1-*ct*Rpl5-*ct*Rpl11 complexes in transport buffer (upper panel) or transport buffer containing cytosol and energy (GTP/ATP) (lower panel) for 30 min at 30ºC. Nuclear translocation of *ct*Syo1 or the *ct*Syo1-containing complexes was revealed by indirect immunofluorescence against Flag-tagged *ct*Syo1. **(C)** BIAcore analysis of the interaction between purified *ct*Syo1 or the *ct*Syo1-*ct*Rpl5, *ct*Syo1-*ct*Rpl11, and *ct*Syo1-*ct*Rpl5-*ct*Rpl11 complexes and the FG-repeat domain of Nup100. GST-Nup100 was immobilized and different concentrations (0.045 - 0.48 μM) of purified *ct*Syo1 or the *ct*Syo1-containing complexes were injected over the sensor chip.

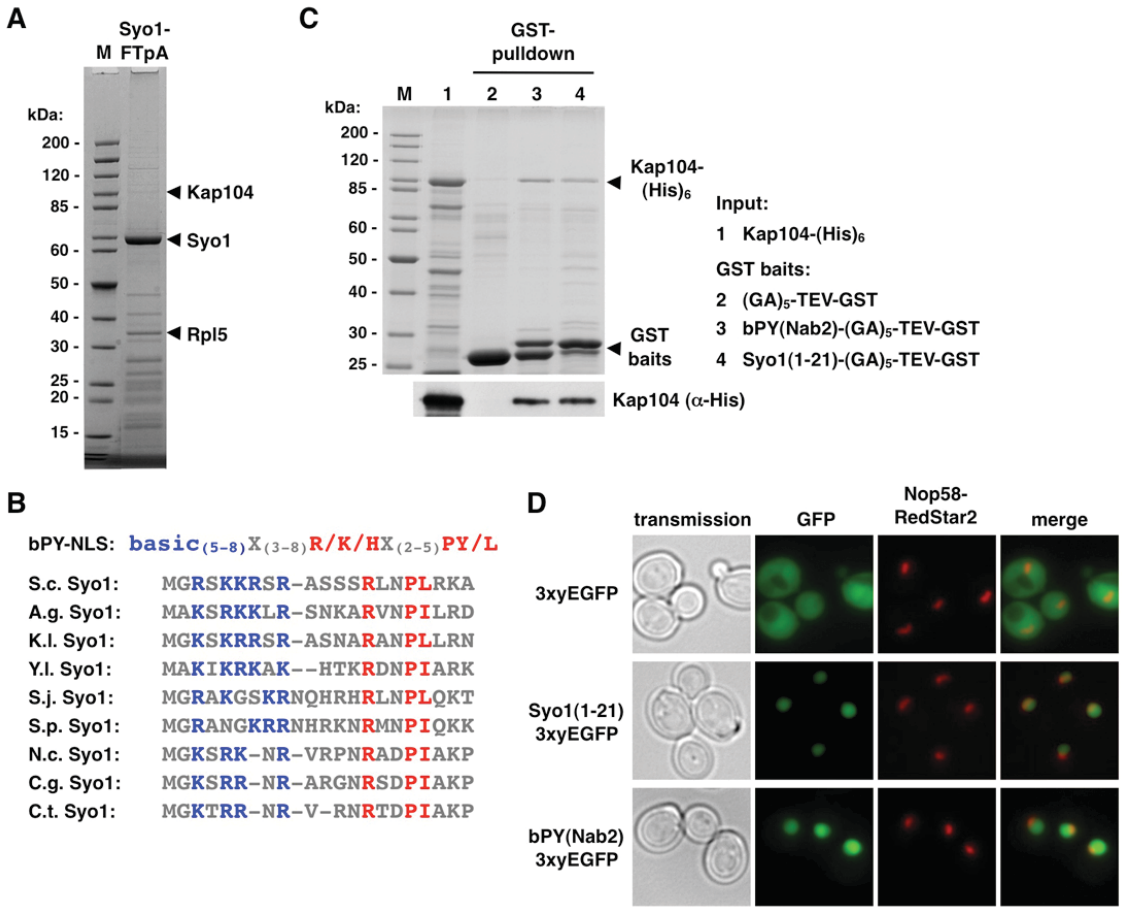

Fig. S11. The PY-NLS of Syo1 is sufficient to mediate interaction with Kap104 and nuclear targeting of a GFP reporter. **(A)** Identification of Kap104 as a Syo1 interacting protein by tandem-affinity purification of C-terminally FTpA-tagged Syo1 from yeast cell lysates. Cells were grown in YPD at 30ºC to an OD_{600} of around 4 and cells were lysed in a buffer containing 50 mM Tris-HCl pH 7.5, 100 mM NaCl, 1.5 mM $MgCl_2$, 5% glycerol, and 0.1% NP-40. The final eluate was analyzed by SDS-PAGE and Coomassie staining. Proteins indicated by arrowheads were identified by mass spectrometry. M, molecular weight standard. Note that the observed differences compared to the purification shown in Fig. 1B are likely due to the different growth (YPD 23ºC, OD_{600} of around 1.2) and purification (same buffer, but 5 mM $MgCl_2$) conditions. **(B)** Syo1 contains a basic PY-NLS at its N-terminus. bPY-NLS, consensus PY-NLS; S.c., *S. cerevisiae*; A.g., *Ashbya gossypii*; K.l., *Kluyveromyces lactis*; Y.l.; *Yarrowia lipolytica*; S.j., *Schizosaccharomyces japonicus*; S.p., *Schizosaccharomyces pombe*; N.c., *Neurospora crassa*; C.g., *Chaetomium globosum*; C.t., *Chaetomium thermophilum*. **(C)** The PY-NLS of Syo1 interacts with Kap104. *In vitro* binding assay between purified Kap104-$(His)_6$ (input, lane 1) and immobilized GST fusion proteins [lane 2, $(GA)_5$-TEV-GST; lane 3, bPY(Nab2)-$(GA)_5$-TEV-GST; lane 4, Syo1(1-21)-$(GA)_5$-TEV-GST]. bPY(Nab2), amino acids 216-242 of Nab2. Bound proteins, eluted from GSH-Sepharose by boiling in sample buffer, were revealed by SDS-PAGE and Coomassie staining (upper panel) or by Western analysis using anti-penta-His antibody (lower panel). M, molecular weight standard. The buffer used for the binding assay had the following composition: 20 mM HEPES pH 7.5, 110 mM K-acetate, 2 mM Mg-acetate, 2 mM EGTA, 20% glycerol, and 1 mM DTT. **(D)** The PY-NLS of Syo1 targets a 3xyEGFP reporter to the

nucleus. bPY(Nab2), amino acids 216-242 of Nab2. Nuclei were revealed by the nucleolar marker protein Nop58-RedStar2.

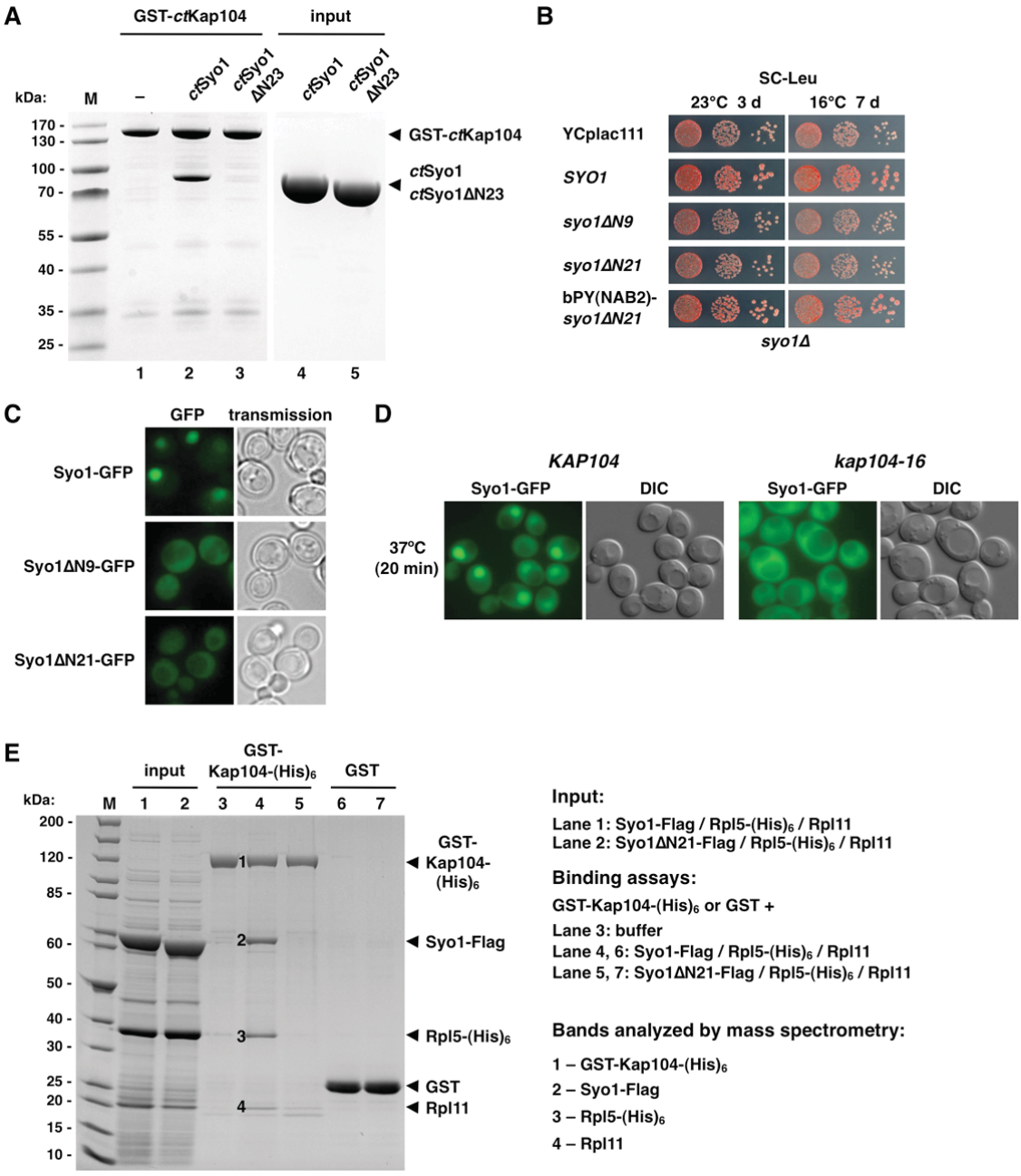

Fig. S12. The PY-NLS of Syo1 is required for nuclear targeting and interaction with Kap104. **(A)** The PY-NLS is required for *in vitro* binding of *ct*Syo1 to *ct*Kap104. *In vitro* binding assay between GST-*ct*Kap104 (lane 1) and *ct*Syo1 (lane 2; input lane 4) or *ct*Syo1ΔN23 (lane 3; input lane 5). Bound proteins were revealed by SDS-PAGE and Coomassie staining. M, molecular weight standard. **(B)** The PY-NLS is essential for Syo1 *in vivo* function. The *syo1Δ* null mutant was transformed with YCplac111, YCplac111-*SYO1*, YCplac111-*syo1ΔN9*, YCplac111-*syo1ΔN21*, and YCplac111-bPY(NAB2)-*syo1ΔN21*. Transformants were restreaked and cells were spotted in 10-fold serial dilution steps onto SC-Leu plates, which were incubated at 23ºC for 3 d or at 16ºC for 7 d. *syo1ΔN9*, Syo1 variant lacking the first 9 residues; *syo1ΔN21*, Syo1 variant lacking the first 21 residues; bPY(NAB2)-*syo1ΔN21*, codes for amino acids 216-242 of Nab2 fused to a Syo1 variant lacking the first 21 residues. **(C)** The PY-NLS is required for nuclear targeting of Syo1. Syo1-GFP,

Syo1ΔN9-GFP, Syo1ΔN21-GFP, and bPY(Nab2)-Syo1ΔN21-GFP were expressed from plasmid under the control of the cognate *SYO1* promoter in *syo1*Δ cells and the localization was assessed by fluorescence microscopy. **(D)** Kap104 is required for nuclear accumulation of Syo1. Localization of chromosomally expressed Syo1-GFP in wild-type (*KAP104*) or temperature-sensitive *kap104-16* mutant (*kap104-16*) cells shifted for 20 min to the non-permissive temperature. DIC, differential interference contrast. **(E)** Syo1-Rpl5-Rpl11 form a trimeric complex that is recruited *via* the PY-NLS of Syo1 to Kap104. *In vitro* binding assay between GST-Kap104-$(His)_6$, immobilized on GSH-Sepharose, and Syo1-Flag/Rpl5-$(His)_6$/Rpl11 or Syo1ΔN21-Flag/Rpl5-$(His)_6$/Rpl11. Trimeric Syo1-Flag/Rpl5-$(His)_6$/Rpl11 (lane 1) or Syo1ΔN21-Flag/Rpl5-$(His)_6$/Rpl11 (lane 2) complexes were obtained by lysing cells having co-expressed Syo1-Flag/Rpl5-$(His)_6$ or Syo1ΔN21-Flag/Rpl5-$(His)_6$ together with cells having expressed Rpl11 followed by Nickel-ion affinity chromatography. Immobilized GST-Kap104-$(His)_6$ was incubated with buffer (lane3), Syo1-Flag/Rpl5-$(His)_6$/Rpl11 (lane 4) or Syo1ΔN21-Flag/Rpl5-$(His)_6$/Rpl11 (lane 5). For control purposes, immobilized GST was incubated with Syo1-Flag/Rpl5-$(His)_6$/Rpl11 (lane 6) or Syo1ΔN21-Flag/Rpl5-$(His)_6$/Rpl11 (lane 7). Bound proteins, eluted from GSH-Sepharose by boiling in sample buffer, were analyzed by SDS-PAGE and Coomassie staining. The identity of the indicated proteins (1-4) was verified by mass spectrometry. M, molecular weight standard. The buffer used for the binding assay had the following composition: 20 mM HEPES pH 8, 150 mM NaCl, 10 mM $MgCl_2$, 10 mM KCl, 1 mM DTT, and 0.1% NP-40.

Table S1. Determination of absolute molecular weights of Syo1 and Syo1-containing complexes.

	Calculated MW	Absolute MW
*ct*Syo1-(His)6	75.6	73.7 ± 0.6 %
(His)6-*ct*Kap104	106.3	106.8 ± 0.4 %
*ct*Syo1-Flag / *ct*Rpl5 / *ct*Rpl11-(His)6	132.8	131.1 ± 0.8 %
*ct*Syo1-Flag / *ct*Rpl5 / *ct*Rpl11-(His)6 / (His)6-*ct*Kap104	239.0	240.0 ± 1.2 %

The absolute molecular weights (MW) were determined from static light scattering (SLS) and refractive index measurements (RI). The MW is given in kDa.

Table S2. Data collection, phasing and refinement statistics.

	*ct*Syo1ΔN23 Se-Met	*ct*Syo1/ *ct*Rpl5-N	*ct*Syo1
Data collection			
Space group	P 1 2_1 1	C 2 2 2_1	C2
Cell dimensions			
a, *b*, *c* (Å)	49.05, 81.27, 83.37	79.6 104.2 182.3	166.4 59.7 69.6
α, β, γ (°)	90.00, 94.97, 90.00	90.00, 90.00, 90.00	90 97.7 90
	Peak		
Energy (keV)	12.6616		
Resolution (Å)	58.09-2.43	63.3-2.95 (3.11 – 2.95)	41.2 – 2.1 (2.21 – 2.1)
R_{merge}	0.087 (0.45) *	0.127 (0.44)	0.078 (0.47)
$I / \sigma I$	21.8 (5.8)	11.2 (4.4)	9.5 (2.6)
Completeness (%)	99.9 (99.3)	100 (100)	99.8 (99.5)
Redundancy	14.5 (14.0)	7.1 (7.2)	3.8 (3.7)
Anomalous completeness	99.8 (98.8)		
Anomalous Redundancy	7.3 (7.1)		
Refinement			
Resolution (Å)	48.8 – 2.4	45.2 – 2.95	40.5 – 2.1
No. reflections	24492	15983	39659
R_{work} / R_{free}	21.7/27.1	20.3/25.9	21.9/25.5
No. atoms			
Protein	4154	4412	4548
Ligand/ion	0	0	0
Water	100	0	218
R.m.s deviations			
Bond lengths (Å)	0.017	0.009	0.008
Bond angles (°)	1.657	1.338	1.105
Ramachandran (%)			
Preferred		94.3	96
Allowed		5.3	3.45
Outliers		0.36	0.55

*Values in parentheses are for highest-resolution shell.

The following amino acid residues could not be resolved due to lacking electron density:
*ct*Syo1: 1 - 24; 326 - 407; 538 - 550
*ct*Syo1-*ct*Rpl5-N: 1 - 33; 328 - 406; 538 - 550

Table S3. Yeast strains used in this study.

Name		Relevant genotype	Source
Y3833	*MAT*α	wild type	This study
Y3834	*MAT*α	*syo1*::natNT2	This study
Y3840*	*MAT*α	*NOP58*-RedStar2::natNT2	This study
Y3877#	*MAT***a**	*rpl5*::kanMX6 pRS315-*RPL5*-TAP *his3 leu2 lys2 ura3 TRP1 MET15*	This study
Y4047	*MAT***a**	*SYO1*-FTpA::HIS3MX4	This study
Y4051	*MAT***a**	*syo1*::natNT2 *ade3*::kanMX4	This study
Y4248	*MAT***a**	*kap104*::natNT2 *SYO1*-GFP::HIS3MX4 *ade3*::kanMX4 pRS316-*KAP104*	This study
Y4462	*MAT***a**	*rpl5*::HIS3MX4 *syo1*::natNT2 *ade3*::kanMX4 pHT4467Δ-*RPL5*	This study
Y4465	*MAT*α	*rpl5*::HIS3MX4 *ade3*::kanMX4 pHT4467Δ-*RPL5*	This study
PJ69-4A#	*MAT***a**	*trp1-901 leu2-3,112 ura3-52 his3-200 gal4*Δ *gal80*Δ *LYS2*::*GAL1-HIS3 GAL2-ADE2 met2*::*GAL7*-lacZ	James *et al.* (*36*)

Strains used in this study were derived from W303 (*MAT***a**/*MAT*α *ade2-1*/*ade2-1 his3-11,15*/*his3-11,15 leu2-3,112*/*leu2-3,112 trp1-1*/*trp1-1 ura3-1*/*ura3-1 can1-100*/*can1-100*) (*32*). Strains derived from DS1-2b (*MAT*α *his3-*Δ*200 leu2-*Δ*1 trp1-*Δ*63 ura3-52*) (*49*) are marked by an asterisk; # indicates strains of other genetic backgrounds.

Table S4. *S. cerevisiae* plasmids used in this study*.

Name	Relevant information	Source
YCplac111-*SYO1*	CEN, *LEU2*, P*SYO1*, T*SYO1*	This study
YCplac22-*SYO1*	CEN, *TRP1*, P*SYO1*, T*SYO1*	This study
YEplac112-*SYO1*	2μ, *TRP1*, P*SYO1*, T*ADH1*	This study
YCplac111-*SYO1*-(GA)5-yEGFP	CEN, *LEU2*, P*SYO1*, T*SYO1*, C-terminal yEGFP	This study
pADH111-$(GA)_5$-3xyEGFP	CEN, *LEU2*, P*ADH1*, T*ADH1*, C-terminal 3xyEGFP	This study
pADH111-*SYO1*(1-21)-$(GA)_5$-3xyEGFP	CEN, *LEU2*, P*ADH1*, T*ADH1*, C-terminal 3xyEGFP	This study
pADH111-bPY(*NAB2*)-$(GA)_5$-3xyEGFP	CEN, *LEU2*, P*ADH1*, T*ADH1*, C-terminal 3xyEGFP	This study
pHT4467Δ(*TRP1*/Δ*URA3*)-*SYO1*	CEN6 (instable), *TRP1*, *ADE3*	This study
pHT4467Δ-*RPL5*	CEN6 (instable), *URA3*, *ADE3*	Hurt lab plasmid
YCplac111-*RPL5*	CEN, *LEU2*, P*RPL5*, T*RPL5*	This study
YEplac181-*RPL5*	2μ, *LEU2*, P*RPL5*, T*RPL5*	This study
YCplac22-*RPL5*	CEN, *TRP1*, P*RPL5*, T*RPL5*	This study
pRS315-RPL5-TAP	CEN, *LEU2*, P*RPL5*, T*GAL4*, C-terminal TAP tag	Hurt lab plasmid
pRS316-*KAP104*	CEN, *URA3*, P*KAP104*, T*KAP104*	Aitchison *et al.* (*31*)
pRS314-*kap104-16*	CEN, *TRP1*, P*KAP104*, T*KAP104*	Aitchison *et al.* (*31*)
pVA3-1	amino acids 72-390 of murine p53 expressed from $pAS1_{CYH2}$; 2μ, *TRP1*, P*ADH1*, N-terminal G4BD	Clontech
pTD1-1	amino acids 87-708 of SV40 large T-antigen expressed from pACT2; 2μ, *LEU2*, P*ADH1*, N-terminal G4AD	Clontech
pG4BDC22-*SYO1*	CEN, *TRP1*, P*ADH1*, T*ADH1*, C-terminal G4BD	This study
pG4BDC22-*ctSYO1*	CEN, *TRP1*, P*ADH1*, T*ADH1*, C-terminal G4BD	This study
pG4BDC(Δmyc)22	CEN, *TRP1*, P*ADH1*, T*ADH1*, C-terminal G4BD(Δmyc)	This study
pG4BDC(Δmyc)22-*SYO1*	CEN, *TRP1*, P*ADH1*, T*ADH1*, C-terminal G4BD(Δmyc)	This study
pG4ADC111-*RPL5*	CEN, *LEU2*, P*ADH1*, T*ADH1*, C-terminal G4AD	This study
pG4ADC111-*ctRPL5*	CEN, *LEU2*, P*ADH1*, T*ADH1*, C-terminal G4AD	This study
pG4ADC181-*RPL11B*	2μ, *LEU2*, P*ADH1*, T*ADH1*, C-terminal G4AD	This study
pGAG4ADC181	2μ, *LEU2*, P*ADH1*, T*ADH1*, C-terminal $(GA)_5$-G4AD	This study
pFA6a-HIS3MX4	for genomic deletion disruption	Longtine *et al.* (*34*)
pFA6a-natNT2	for genomic deletion disruption	Janke *et al.* (*33*)
pFA6a-GFP-HIS3MX4	GFP(S65T), T*ADH1*; for genomic C-terminal tagging	Longtine *et al.* (*34*)
pFA6a-FTpA-HIS3MX4	FTpA, T*ADH1*; for genomic C-terminal tagging	This study
pFA6a-RedStar2-natNT2	pYM43; RedStar2; for genomic C-terminal tagging	Janke *et al.* (*33*)

*For simplicity, only the plasmids containing wild-type *SYO1*, *RPL5*, and *KAP104* are listed; variants/mutants thereof were cloned into the listed plasmids. P and T denote promoter and terminator, respectively.

Table S5. *E. coli* expression plasmids used in this study*.

Name	Relevant information	Source
pET-15b/SYO1-$(His)_6$	amp^r, T7 promoter/*lac* operator	This study
pET-22b/SYO1-2xyEGFP-$(His)_6$	amp^r, T7 promoter/*lac* operator	This study
pETDuet-1/RPL5-$(His)_6$-SYO1	amp^r, T7 promoter/*lac* operator	This study
pETDuet-1/RPL5-$(His)_6$-SYO1-Flag	amp^r, T7 promoter/*lac* operator	This study
pET-24d/$(GA)_5$-TEV-GST	kan^r, T7 promoter/*lac* operator	This study
pET-24d/SYO1(1-21)-$(GA)_5$-TEV-GST	kan^r, T7 promoter/*lac* operator	This study
pET-24d/bPY(NAB2)-$(GA)_5$-TEV-GST	kan^r, T7 promoter/*lac* operator	This study
pET-15b/*ct*SYO1	amp^r, T7 promoter/*lac* operator	This study
pET-15b/*ct*SYO1-$(His)_6$	amp^r, T7 promoter/*lac* operator	This study
pET-15b/*ct*SYO1-Flag-$(His)_6$	amp^r, T7 promoter/*lac* operator	This study
pETDuet-1/*ct*RPL5-$(His)_6$-*ct*SYO1	amp^r, T7 promoter/*lac* operator	This study
pETDuet-1/*ct*RPL5-*ct*SYO1-Flag	amp^r, T7 promoter/*lac* operator	This study
pET-24d/RPL11B	kan^r, T7 promoter/*lac* operator	This study
pET-24d/*ct*RPL11	kan^r, T7 promoter/*lac* operator	This study
pET-24d/*ct*RPL11-$(His)_6$	kan^r, T7 promoter/*lac* operator	This study
pET-15b/KAP104-$(His)_6$	amp^r, T7 promoter/*lac* operator	This study
pET-24d/GST-TEV-$(GA)_5$	kan^r, T7 promoter/*lac* operator	This study
pET-24d/GST-TEV-$(GA)_5$-KAP104-$(His)_6$	kan^r, T7 promoter/*lac* operator	This study
pET-24d/GST-TEV-$(His)_6$-*ct*KAP104	kan^r, T7 promoter/*lac* operator	This study
pET-24d/$(His)_6$-*ct*KAP104	kan^r, T7 promoter/*lac* operator	This study
pProEX/$(His)_6$-TEV-*ct*GSP1	amp^r, *trc* promoter	This study
pGEX-2TK-NUP100(1-640)	amp^r, *tac* promoter	Allen *et al.* (*50*)
pGEX-2TK-NUP116(165-715)	amp^r, *tac* promoter	Allen *et al.* (*50*)
pGEX-2TK-NUP1(332-1076)	amp^r, *tac* promoter	Allen *et al.* (*50*)
pGEX-2T/NLS-RFP	amp^r, *tac* promoter, GST-SV40NLS-mRFP	Yoneda lab plasmid

*For simplicity, only the plasmids containing wild-type *SYO1* or *RPL5* are listed; variants/mutants thereof were cloned into the listed plasmids.

ferences and Notes

F. M. Boisvert, S. van Koningsbruggen, J. Navascués, A. I. Lamond, The multifunctional nucleolus. *Nat. Rev. Mol. Cell Biol.* **8**, 574 (2007). doi:10.1038/nrm2184 Medline

D. L. Lafontaine, D. Tollervey, The function and synthesis of ribosomes. *Nat. Rev. Mol. Cell Biol.* **2**, 514 (2001). doi:10.1038/35080045 Medline

T. Pederson, R. Y. Tsai, In search of nonribosomal nucleolar protein function and regulation. *J. Cell Biol.* **184**, 771 (2009). doi:10.1083/jcb.200812014 Medline

J. R. Warner, The economics of ribosome biosynthesis in yeast. *Trends Biochem. Sci.* **24**, 437 (1999). doi:10.1016/S0968-0004(99)01460-7 Medline

A. K. Henras *et al.*, The post-transcriptional steps of eukaryotic ribosome biogenesis. *Cell. Mol. Life Sci.* **65**, 2334 (2008). doi:10.1007/s00018-008-8027-0 Medline

D. Kressler, E. Hurt, J. Bassler, Driving ribosome assembly. *Biochim. Biophys. Acta* **1803**, 673 (2010). doi:10.1016/j.bbamcr.2009.10.009 Medline

J. P. Staley, J. L. Woolford Jr., Assembly of ribosomes and spliceosomes: Complex ribonucleoprotein machines. *Curr. Opin. Cell Biol.* **21**, 109 (2009). doi:10.1016/j.ceb.2009.01.003 Medline

H. Tschochner, E. Hurt, Pre-ribosomes on the road from the nucleolus to the cytoplasm. *Trends Cell Biol.* **13**, 255 (2003). doi:10.1016/S0962-8924(03)00054-0 Medline

Y. M. Chook, K. E. Süel, Nuclear import by karyopherin-βs: Recognition and inhibition. *Biochim. Biophys. Acta* **1813**, 1593 (2011). doi:10.1016/j.bbamcr.2010.10.014 Medline

. M. P. Rout, G. Blobel, J. D. Aitchison, A distinct nuclear import pathway used by ribosomal proteins. *Cell* **89**, 715 (1997). doi:10.1016/S0092-8674(00)80254-8 Medline

. D. Görlich, U. Kutay, Transport between the cell nucleus and the cytoplasm. *Annu. Rev. Cell Dev. Biol.* **15**, 607 (1999). Medline

. M. Stewart, Molecular mechanism of the nuclear protein import cycle. *Nat. Rev. Mol. Cell Biol.* **8**, 195 (2007). doi:10.1038/nrm2114 Medline

. A. Ben-Shem *et al.*, The structure of the eukaryotic ribosome at 3.0 Å resolution. *Science* **334**, 1524 (2011). doi:10.1126/science.1212642 Medline

. S. Ferreira-Cerca *et al.*, Analysis of the in vivo assembly pathway of eukaryotic 40S ribosomal proteins. *Mol. Cell* **28**, 446 (2007). doi:10.1016/j.molcel.2007.09.029 Medline

. G. Pöll *et al.*, rRNA maturation in yeast cells depleted of large ribosomal subunit proteins. *PLoS ONE* **4**, e8249 (2009). doi:10.1371/journal.pone.0008249 Medline

. M. Ciganda, N. Williams, Eukaryotic 5S rRNA biogenesis. *Wiley Interdiscip. Rev. RNA* **2**, 523 (2011). doi:10.1002/wrna.74 Medline

. M. Claussen, F. Rudt, T. Pieler, Functional modules in ribosomal protein L5 for ribonucleoprotein complex formation and nucleocytoplasmic transport. *J. Biol. Chem.* **274**, 33951 (1999). doi:10.1074/jbc.274.48.33951 Medline

. J. Zhang *et al*., Assembly factors Rpf2 and Rrs1 recruit 5S rRNA and ribosomal proteins rpL5 and rpL11 into nascent ribosomes. *Genes Dev.* **21**, 2580 (2007). doi:10.1101/gad.1569307 Medline

. S. Amlacher *et al*., Insight into structure and assembly of the nuclear pore complex by utilizing the genome of a eukaryotic thermophile. *Cell* **146**, 277 (2011). doi:10.1016/j.cell.2011.06.039 Medline

. M. A. Andrade, C. Petosa, S. I. O'Donoghue, C. W. Müller, P. Bork, Comparison of ARM and HEAT protein repeats. *J. Mol. Biol.* **309**, 1 (2001). doi:10.1006/jmbi.2001.4624 Medline

. D. Xu, A. Farmer, Y. M. Chook, Recognition of nuclear targeting signals by Karyopherin-β proteins. *Curr. Opin. Struct. Biol.* **20**, 782 (2010). doi:10.1016/j.sbi.2010.09.008 Medline

. K. E. Süel, A. E. Cansizoglu, Y. M. Chook, Atomic resolution structures in nuclear transport *Methods* **39**, 342 (2006). doi:10.1016/j.ymeth.2006.06.015 Medline

. M. Marfori *et al*., Molecular basis for specificity of nuclear import and prediction of nuclear localization. *Biochim. Biophys. Acta* **1813**, 1562 (2011). doi:10.1016/j.bbamcr.2010.10.013 Medline

. Y. Matsuura, M. Stewart, Nup50/Npap60 function in nuclear protein import complex disassembly and importin recycling. *EMBO J.* **24**, 3681 (2005). doi:10.1038/sj.emboj.7600843 Medline

. R. Bayliss, T. Littlewood, L. A. Strawn, S. R. Wente, M. Stewart, GLFG and FxFG nucleoporins bind to overlapping sites on importin-beta. *J. Biol. Chem.* **277**, 50597 (2002). doi:10.1074/jbc.M209037200 Medline

. S. A. Adam, R. S. Marr, L. Gerace, Nuclear protein import in permeabilized mammalian cells requires soluble cytoplasmic factors. *J. Cell Biol.* **111**, 807 (1990). doi:10.1083/jcb.111.3.807 Medline

. B. Bradatsch *et al*., Arx1 functions as an unorthodox nuclear export receptor for the 60S preribosomal subunit. *Mol. Cell* **27**, 767 (2007). doi:10.1016/j.molcel.2007.06.034 Medline

. F. R. Bischoff, C. Klebe, J. Kretschmer, A. Wittinghofer, H. Ponstingl, RanGAP1 induces GTPase activity of nuclear Ras-related Ran. *Proc. Natl. Acad. Sci. U.S.A.* **91**, 2587 (1994). doi:10.1073/pnas.91.7.2587 Medline

. B. J. Lee *et al*., Rules for nuclear localization sequence recognition by karyopherin beta 2. *Cell* **126**, 543 (2006). doi:10.1016/j.cell.2006.05.049 Medline

. K. E. Süel, H. Gu, Y. M. Chook, Modular organization and combinatorial energetics of proline-tyrosine nuclear localization signals. *PLoS Biol.* **6**, e137 (2008). doi:10.1371/journal.pbio.0060137 Medline

. J. D. Aitchison, G. Blobel, M. P. Rout, Kap104p: A karyopherin involved in the nuclear transport of messenger RNA binding proteins. *Science* **274**, 624 (1996). doi:10.1126/science.274.5287.624 Medline

. B. J. Thomas, R. Rothstein, Elevated recombination rates in transcriptionally active DNA. *Cell* **56**, 619 (1989). doi:10.1016/0092-8674(89)90584-9 Medline

. C. Janke *et al*., A versatile toolbox for PCR-based tagging of yeast genes: New fluorescent proteins, more markers and promoter substitution cassettes. *Yeast* **21**, 947 (2004). doi:10.1002/yea.1142 Medline

. M. S. Longtine *et al*., Additional modules for versatile and economical PCR-based gene deletion and modification in *Saccharomyces cerevisiae*. *Yeast* **14**, 953 (1998). doi:10.1002/(SICI)1097-0061(199807)14:10<953::AID-YEA293>3.0.CO;2-U Medline

. D. Kressler, M. Doère, M. Rojo, P. Linder, Synthetic lethality with conditional dbp6 alleles identifies rsa1p, a nucleoplasmic protein involved in the assembly of 60S ribosomal subunits. *Mol. Cell. Biol.* **19**, 8633 (1999). Medline

. P. James, J. Halladay, E. A. Craig, Genomic libraries and a host strain designed for highly efficient two-hybrid selection in yeast. *Genetics* **144**, 1425 (1996). Medline

. Collaborative Computational Project, Number 4, The CCP4 suite: Programs for protein crystallography. *Acta Crystallogr. D Biol. Crystallogr.* **50**, 760 (1994). doi:10.1107/S0907444994003112 Medline

. P. D. Adams *et al*., PHENIX: A comprehensive Python-based system for macromolecular structure solution. *Acta Crystallogr. D Biol. Crystallogr.* **66**, 213 (2010). doi:10.1107/S0907444909052925 Medline

. P. Emsley, K. Cowtan, Coot: Model-building tools for molecular graphics. *Acta Crystallogr. D Biol. Crystallogr.* **60**, 2126 (2004). doi:10.1107/S0907444904019158 Medline

. S. R. Price, N. Ito, C. Oubridge, J. M. Avis, K. Nagai, Crystallization of RNA-protein complexes. I. Methods for the large-scale preparation of RNA suitable for crystallographic studies. *J. Mol. Biol.* **249**, 398 (1995). doi:10.1006/jmbi.1995.0305 Medline

. K. Wild *et al*., Structural insights into the assembly of the human and archaeal signal recognition particles. *Acta Crystallogr. D Biol. Crystallogr.* **66**, 295 (2010). doi:10.1107/S0907444910000879 Medline

. W. Rist, C. Graf, B. Bukau, M. P. Mayer, Amide hydrogen exchange reveals conformational changes in hsp70 chaperones important for allosteric regulation. *J. Biol. Chem.* **281**, 16493 (2006). doi:10.1074/jbc.M600847200 Medline

. W. Rist, T. J. Jørgensen, P. Roepstorff, B. Bukau, M. P. Mayer, Mapping temperature-induced conformational changes in the *Escherichia coli* heat shock transcription factor sigma 32 by amide hydrogen exchange. *J. Biol. Chem.* **278**, 51415 (2003). doi:10.1074/jbc.M307160200 Medline

. Z. Zhang, C. B. Post, D. L. Smith, Amide hydrogen exchange determined by mass spectrometry: Application to rabbit muscle aldolase. *Biochemistry* **35**, 779 (1996). doi:10.1021/bi952227q Medline

. D. Kressler, J. de la Cruz, M. Rojo, P. Linder, Fal1p is an essential DEAD-box protein involved in 40S-ribosomal-subunit biogenesis in *Saccharomyces cerevisiae*. *Mol. Cell. Biol.* **17**, 7283 (1997). Medline

. D. Kressler, D. Roser, B. Pertschy, E. Hurt, The AAA ATPase Rix7 powers progression of ribosome biogenesis by stripping Nsa1 from pre-60S particles. *J. Cell Biol.* **181**, 935 (2008). doi:10.1083/jcb.200801181 Medline

. M. Deshmukh, J. Stark, L. C. Yeh, J. C. Lee, J. L. Woolford Jr., Multiple regions of yeast ribosomal protein L1 are important for its interaction with 5 S rRNA and assembly into ribosomes. *J. Biol. Chem.* **270**, 30148 (1995). doi:10.1074/jbc.270.50.30148 Medline

. L. J. McGuffin, K. Bryson, D. T. Jones, The PSIPRED protein structure prediction server. *Bioinformatics* **16**, 404 (2000). doi:10.1093/bioinformatics/16.4.404 Medline

. T. A. Nissan, J. Bassler, E. Petfalski, D. Tollervey, E. Hurt, 60S pre-ribosome formation viewed from assembly in the nucleolus until export to the cytoplasm. *EMBO J.* **21**, 5539 (2002). doi:10.1093/emboj/cdf547 Medline

. N. P. Allen, L. Huang, A. Burlingame, M. Rexach, Proteomic analysis of nucleoporin interacting proteins. *J. Biol. Chem.* **276**, 29268 (2001). doi:10.1074/jbc.M102629200 Medline